 ©2003 Kvantovaya Elektronika and Turpion Ltd

PACS numbers: 42.55.Px; 42.60.Lh
DOI: 10.1070/QE2003v033n01ABEH002364

Threshold and efficiency of a laser cathode-ray tube at room temperature

V.I. Kozlovsky, Yu.M. Popov

***Abstract*. The main factors determining the lasing threshold and efficiency of a laser cathode-ray tube at room temperature are considered. Recent achievements obtained by using laser screens made of the II – VI compound single crystals are discussed. It is shown that multilayer heterostructures allow the reduction in the lasing threshold by several times.**

Keywords: *laser cathode-ray tube, heterostructures, semiconductor laser.*

1. Introduction

A laser cathode-ray tube (LCRT) was one of the most promising inventions in the field of electron-beam-pumped semiconductor lasers [1]. However, thirty years have already elapsed after the first reports on the experimental implementation of LCRTs [2, 3] but this invention has not found so far wide applications in practice because of the absence of laser screens (LSs) that could efficiently work at room and higher temperatures. In this paper, we discuss briefly recent results obtained in this field and propose a number of ways to improve the characteristics of LSs such as the lasing threshold and efficiency, and the output power.

2. Lasing threshold in a LCRT with a single-crystal active element

Upon uniform excitation of a semiconductor crystal by an electron beam of diameter d_e, the current density j_e, and the penetration depth z_0, which depends on the electron energy E_e, the volume concentration n of nonequilibrium current carriers can be estimated from the expression

$$n = \frac{j_e E_e k_1 \tau}{e z_0 \varepsilon_{eh}}, \qquad (1)$$

where k_1 is the coefficient characterising the fraction of the electron-beam energy that is absorbed inside the semiconductor crystal; τ is the lifetime of nonequilibrium carriers in the excited region; e is the electron charge; $\varepsilon_{eh} \approx 3E_g$ is the energy required to generate one electron – hole pair; and E_g is the energy gap. The intensity of spontaneous emission can be found from the expression [4]

$$\frac{n}{\tau} \approx \frac{\mu_0^{1.5}\varepsilon_0^{0.5} N}{\pi\hbar^4}\int_{E_g}^{\infty}\langle R_{ch}^2\rangle E^3 \rho_{cv}(E) f_c(E) f_v(E)\,\mathrm{d}E, \qquad (2)$$

where μ_0 is the magnetic constant of vacuum; ε_0 is the dielectric constant of vacuum; N is the refractive index; f_c and f_v are the Fermi distribution functions for electrons and holes in the conduction and valence bands, respectively. The density of states ρ_{cv} and the square of the dipole moment $\langle R_{ch}^2\rangle$ are described by the expressions

$$\rho_{cv}(E) = \frac{1}{2\pi^2\hbar^3}\left(\frac{2m_e m_h}{m_e + m_h}\right)^{3/2}(E - E_g)^{1/2}, \qquad (3)$$

$$\langle R_{ch}^2\rangle = \frac{\hbar^2 e^2}{6 m_e E^2}\left(\frac{m_0}{m_e} - 1\right)\frac{E_g(E_g + \Delta)}{E_g + 2\Delta/3}, \qquad (4)$$

where m_e and m_h are the effective masses of an electron and a hole in the conduction and valence bands, respectively; m_0 is the electron mass; and Δ is the spin – orbit splitting energy. Expression (2) was derived assuming that radiative recombination is determined by direct transitions between the conduction and valence bands, and expression (4) was derived assuming that the active region of the laser represents an isotropic crystal with a lattice of the sphalerite type.

In expression (1) relating the electron-beam current density to the concentration of nonequilibrium carriers, it is most difficult to determine the lifetime τ. The calculation using expressions (2) – (4) for ZnSe with parameters $m_e = 0.17m_0$, $m_h = 0.6m_0$, $\Delta = 0.43$ eV, $E_g = 2.65$ eV, $N = 2.85$ [5] and $T = 300$ K shows that τ changes from 0.6 to 0.4 ns when n increases from 5×10^{18} to 10^{19} cm^{-3}. A similar calculation for CdS for $m_e = 0.205m_0$, $m_h = 1.35m_0$, $\Delta = 0.065$ eV, $E_g = 2.39$ eV, $N = 2.8$, and $T = 300$ K gives the change in τ from 2.9 to 1.6 ns with increasing n from 5×10^{18} to 10^{19} cm^{-3}. The method for measuring the lifetime of carriers at the lasing threshold directly in the LCRT was described in Ref. [6]. This method gives $\tau = 3$ ns for CdSSe LSs at room temperature.

To explain the characteristics of lasers based on high energy-gap II – VI compounds, several models of the optical gain were proposed [4, 7 – 11]. These models can be conditionally divided into two groups. The models of the first group are based on the fact that the gain is related to the recombination of excitons. This is either the recombination

V.I. Kozlovsky, Yu.M. Popov P.N. Lebedev Physics Institute, Russian Academy of Sciences, Leninsky prosp. 53, 119991 Moscow, Russia

Received 6 November 2002
Kvantovaya Elektronika **33** (1) 48 – 56 (2003)
Translated by M.N. Sapozhnikov

of a free exciton accompanied by the recoil of the momentum to a phonon, an electron, or other exciton [8] or recombination from a localised state of an exciton [7, 10]. The models of the second group consider transitions in an electron – hole plasma [4, 10, 11]. The exciton mechanisms of optical gain operate mainly at low temperatures and give relatively low gains. An increase in the gain is caused by a transition of the exciton gas to an electron – hole plasma with increasing the excitation intensity (the Mott transition [12]). Because the estimated threshold concentration of nonequilibrium carriers in the LCRT at room temperature greatly exceeds the concentration during the Mott transition, lasing is attributed to transitions in a degenerate electron – hole plasma [11].

The simplest model describing amplification in an electron – hole plasma is based on the fact that the interaction between particles in a dense plasma weakly affects the gain, which can be calculated taking into account the interband transitions in the band model of a semiconductor. However, this interaction results in the narrowing of the energy gap [11]. In this case, the gain can be written in the form [4]

$$g(\omega) = \left(\frac{\mu_0}{\varepsilon_0}\right)^{1/2}\left(\frac{\omega}{N}\right)\int_{E_g}^{\infty}\langle R_{\text{ch}}^2\rangle\rho_{\text{cv}}(E)[f_{\text{c}}(E)+f_{\text{v}}(E)-1] \times \frac{\hbar/\tau_{\text{in}}}{(E-\hbar\omega)^2+(\hbar/\tau_{\text{in}})^2}\,\text{d}E, \quad (5)$$

where τ_{in} is the time of intraband relaxation. The latter factor in the integrand, which describes the line shape, can be replaced by the delta function in the simplest case of direct interband transitions [13]. This factor should be introduced to explain the absence of a sharp absorption or gain edge in real crystals. The presence of the long-wavelength edge in the absorption or gain spectra in the II – VI compound crystals is attributed to a strong electron – phonon interaction [14, 15]. However, it seems that the effect of this interaction on the maximum of the gain line can be neglected.

A further analysis of expression (5) shows that the dependence of $g_{\max}$ on the concentration n of nonequilibrium carriers at room temperature in the range of g from zero to 1000 cm^{-1} can be approximated with an accuracy $\sim 5\,\%$ by a linear dependence

$$g_{\max}(n) = A(n-n_0), \quad (6)$$

where n_0 is the inversion concentration; A is the differential gain or the cross section for the stimulated transition. For $Zn_{0.8}Cd_{0.2}Se$, the gain $A = 2.5\times10^{-16}$ cm^2 and weakly depends on the intraband relaxation [4]. However, the value of n_0 strongly depends on τ_{in}. When τ_{in} decreases down to 10^{-14} s, the concentration n_0 is approximately doubled. The temperature dependence of n_0 has the form

$$n_0(T) = n_0(T_1)(T/T_1)^{3/2}. \quad (7)$$

The slope of this dependence at $T = 300$ K corresponds to the slope of the dependence

$$j_{\text{th}}(T) = j_{\text{th}}(T_1)\exp[(T-T_1)/T_0], \quad (8)$$

with the characteristic temperature $T_0 = 200$ K. Expression (8) is frequently used to estimate the temperature dependence of the threshold current density for an injection laser, and a similar expression can be applied to approximate expression (7). Because the threshold concentration in a laser is always higher than the inversion concentration, it should be expected that the temperature dependence of the lasing threshold with the characteristic temperature $T_0 >$ 200 K will take place in the LCRT if the resonator losses are independent of temperature. Fig. 1a shows a typical temperature dependence of the threshold current for the CdS LS, for which $T_0 = 140$ K. However, a similar dependence for the current density (Fig. 1b), calculated taking into account a change in the electron-spot diameter with changing current, is more flat, giving $T_0 = 200$ K, which is close to the estimate obtained from expressions (7) and (8).

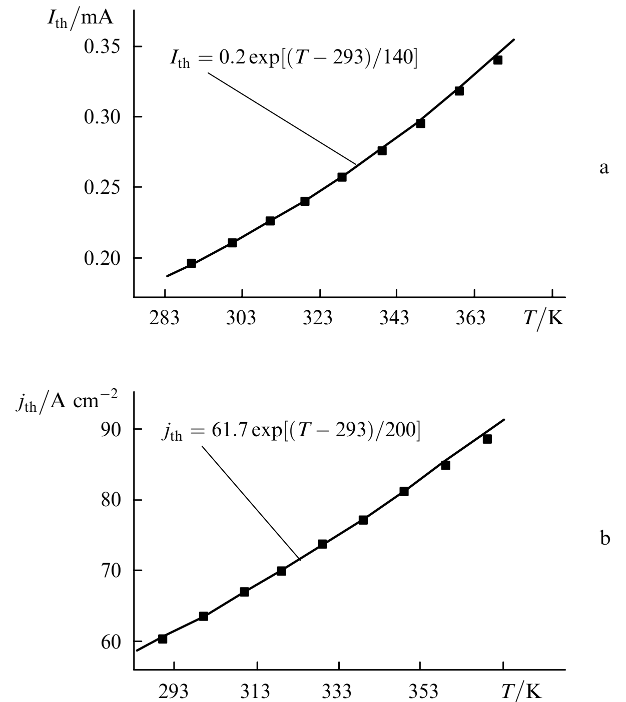

Figure 1. Temperature dependences of the threshold current I_{th} (a) and the threshold current density j_{th} calculated from the threshold current taking into account the dependence of the electron-beam diameter on the current (b).

We will estimate the dependence of the energy gap on n from the empirical expression

$$\Delta E_g = -A_1 n^{1/3}, \quad (9)$$

where A_1 is a constant. By using the data from [16] for ZnSe at 300 K, we find $A_1 = (4-4.5)\times10^{-8}$ eV cm. For $n = 10^{19}$ cm^{-3}, the energy gap narrows down by 90 meV.

In the geometric optics approximation, the threshold condition for lasing at one of the longitudinal modes ω of the resonator upon uniform pumping can be written in the form

$$g(\omega)z_0 = \alpha_a(\omega)z_0 + \alpha_p(\omega)(L_c - z_0) + 0.5|\ln(R_1R_2)|, \quad (10)$$

where α_a, α_p are the coefficients of losses in the active (excited) and passive regions of a semiconductor plate,

respectively; L_c is the resonator length equal to the thickness of the semiconductor plate; R_1 and R_2 are the reflection coefficients of mirror coatings deposited on the plate surfaces. We assume here that the resonator losses can be frequency-dependent, and equality (10) is fulfilled only for one of the resonator modes. The nonuniformity of excitation of the active element in the LCRT along the resonator axis (z axis) can be taken into account by replacing equation (10) by an integral equation of the type

$$\int_0^{L_c} [g(\omega, z) - \alpha(\omega, z)]dz = 0.5|\ln(R_1 R_2)|, \qquad (11)$$

where α is the overall loss coefficient. The transverse nonuniformity of excitation can be taken into account by solving the wave equation with the inhomogeneous complex dielectric constant of a semiconductor [17]. In this case, when the distribution of nonequilibrium carriers perpendicular to the optical axis of the resonator is inhomogeneous, expression (10) can be transformed to

$$g_{\max} z_0 = \Lambda[\alpha L_c + 0.5|\ln(R_1 R_2)|], \qquad (12)$$

where Λ is the parameter of configuration losses [18]. The configuration losses depend on the effective Fresnel number $4\lambda L_c/(N d_e^2)$ (where d_e is the electron-spot diameter) and other losses. Unfortunately, the problem becomes greatly complicated when both the transverse and longitudinal inhomogeneities are taken into account. This was done qualitatively in the geometric optics approximation in Ref. [19], where the radiation pattern of the LCRT was analysed for different operating regimes.

Let us now estimate the lasing threshold at $T = 300$ K. According to [20], the intracavity losses for the CdS LS of thickness $L_c = 15$ μm with the effective reflection of mirrors $R_1 R_2 = 0.9$ are $\alpha = 25$ cm^{-1} at room temperature. For the electron spot of diameter $d_e = 15$ μm, the configuration losses are $\Lambda = 1.5$ [17]. For excitation by 50-keV electrons ($z_0 = 5$ μm), we obtain from (12) the gain $g = 300$ cm^{-1}. By substituting this value into expression (6) and assuming that the cross section A for CdS is approximately the same as for ZnCdSe and $n_0 = 6 \times 10^{18}$ cm^{-3} [11], we obtain the estimate of the threshold concentration of nonequilibrium carriers $n_{th} = 7.2 \times 10^{18}$ cm^{-3}. This value exceeds n_0 only by 20 %.

Then, by substituting the found value of n_{th} into (1) and assuming that the CdS parameters are $k_1 = 0.75$, $E_e = 50$ keV, $z_0 = 5$ μm, $\tau = 2$ ns, and $E_g = 2.5$ eV, we estimate the threshold current density of the electron beam as $j_{th} = 58$ A cm^{-2}. For $d_e = 25$ μm, this value corresponds to the threshold current $I_{th} = 0.28$ mA. These estimates are very close to experimental values. Because the LCRT is mainly used in projection systems, which require a high contrast and many gradations of illumination, it should operate well above the threshold. This causes the first difficulty of the commercial applications of LCRTs due to the necessity of the development of special CRTs with the electron-beam current density of a few hundreds A cm^{-2}. This is especially difficult to realise at small diameters of the electron beam and low accelerating voltages. The main problem at low energies E_e is the retaining of a constant electron-beam diameter d_e during a change in the total current. Otherwise, at the apparent high excess over the threshold current (for example, $I = 2$ mA and $I_{th} = 0.28$ mA), the real excess over the threshold current density will be substantially lower [21].

It was found in Ref. [22] that the total current lasing threshold at low temperature (80 K) increases approximately linearly with increasing diameter of an electron beam from 10 to at least 60 μm. This means that the threshold current density j_{th} decreases as $\sim d_e^{-1}$. Similar data at room temperature are absent. However, it was shown in Ref. [23] that the lasing threshold of the CdS LS is $j_{th} = 20$ A cm^{-2} for $d_e = 70 - 100$ μm, which is approximately three times lower than estimates obtained for small values of d_e. These data have not been adequately explained so far. Indeed, for large diameters $d_e > d_1 \approx 100$ μm, the threshold current density should increase due to the drop of nonequilibrium carriers caused by amplified spontaneous noise [18]. For small diameters $d_e < d_2 \approx 20$ μm (of course, d_2 depends on the resonator length), the threshold current density should increase due to the increase in configuration losses. However, it is difficult to explain the observed change in j_{th} in the region $d_e = 20 - 100$ μm only by configuration losses because the threshold weakly depends on the change of losses in the laser.

Upon a change in the electron-beam diameter in expression (1), only the parameter τ can change along with the threshold concentration. As d_e is increased, the lifetime of nonequilibrium carriers should increase compared to the lifetime of carriers determined by spontaneous emission because a photon of spontaneous emission can be absorbed again in the excited region with the creation of a nonequilibrium electron-hole pair. Such an effect was observed in the III–V heterostructures [24], and its influence on the lasing threshold was discussed in Ref. [25].

However, although an increase in d_e reduces the threshold current density, to achieve the high resolution of the LCRT, the size of the LS and the tube as a whole should be increased, and a more complicated projection optics should be used. We will show below that a substantial decrease in the lasing threshold in the LCRT should be expected when multilayer heterostructures are used as the active element.

3. Lasing threshold in the LCRT with an active element based on a multilayer heterostructure

We pointed out in Section 2 that the lasing threshold is determined first of all by the concentration on inversion of excited carriers, which can be achieved at room temperature in a greater part of the excited region of spatially homogeneous semiconductors only at high electron-beam current densities. However, the studies of injection lasers have shown that, when heterostructures are used, the main part of excited carriers can be concentrated within limited regions [26]. In the case of electron-beam-pumped lasers, it is necessary to fabricate such a structure that would provide the concentration of nonequilibrium carriers in a volume that is smaller than the semiconductor volume initially excited by the electron beam [27]. This structure should be spatially inhomogeneous and should contain a certain number of potential wells to which nonequilibrium carriers can diffuse. In this case, the concentration of carriers in the wells increases proportionally to the ratio of the initially excited volume to the volume occupied by the wells.

The configurations of the potential wells can be different: a layer structure, structures containing wire potential wells or wells confined in all three dimensions (dots). The distance between the wells should be smaller than the doubled diffusion length to provide the efficient concen-

tration of carriers. It was found that the diffusion length for the ZnCdSe/ZnSe layer structure was ~ 0.2 μm [28]. This value is an order of magnitude smaller than the characteristic dimensions of the semiconductor region excited by the electron beam in the LCRT. Therefore, the active region of the laser should contain at least ten potential wells, and their orientation with respect to the optical axis of the resonator can be arbitrary. The multilayer structure with the layers oriented perpendicular to the optical axis of the resonator is the simplest from the technological point of view. To provide the required tenfold decrease in the lasing threshold, the thickness of the layers forming the potential wells should be ten times smaller than the doubled diffusion length, i.e., smaller than 40 nm.

In the case of a homogeneous active medium, the amplification per round trip in the resonator at the lasing threshold is $A(n_{\rm th} - n_0)z_0$ [see (6)]. If the active medium consists of m potential wells, the amplification per round trip in the resonator is $A[n_{\rm th}^{\rm w} z_0/(mL_{\rm w}) - n_0]mL_{\rm w}$, where $L_{\rm w}$ is the well width, and $n_{\rm th}$ and $n_{\rm th}^{\rm w}$ are the threshold concentrations of nonequilibrium carriers, which are averaged over the excited region and are related to the threshold current density of the electron beam by expression (1). The resonator losses being the same, we obtain that the lasing threshold in a laser with the active region containing m potential wells is lower than that in a laser with the homogeneous active medium by a factor of $n_{\rm th}/n_{\rm th}^{\rm w} = [(n_{\rm th} - n_0)/n_{\rm th} + n_0 mL_{\rm w}/(n_{\rm th} z_0)]^{-1}$. For the case considered above, when $n_{\rm th} = 7.2 \times 10^{18}$ cm^{-3}, $n_0 = 6 \times 10^{18}$ cm^{-3}, $m = 10$, $L_{\rm w} = 40$ nm, and $z_0 = 5$ μm, we obtain the reduction in the lasing threshold by a factor of 4.3. By decreasing the resonator losses, we can further decrease the lasing threshold by an order of magnitude.

The quality of a structure depends first of all on the presence of structural defects. To avoid the formation of misfit dislocations during the growth of a layer on a substrate made of another material, the periods of the lattices of the active layer and substrate should be well matched. The matching accuracy $\Delta a/a$ for a structure with a single layer of thickness $L_{\rm w} = 40$ nm should be no worse than 0.006 [29]. In a structure containing ten quantum wells, the elastic stresses from each of the wells will be accumulated, and therefore the matching accuracy should be almost an order of magnitude better. Because the mismatch of the lattice periods for the binary II–VI compounds forming solid solutions is within 0.05–0.07, the growth of the required structure with the well width $L_{\rm w} = 40$ nm is a complicated technological problem. The choice of materials that can be used for solving this problem is rather limited. Another problem is that high-quality substrates matched over the crystal lattice period are required for the epitaxial growth of such structures. The structures can be fabricated from ZnSSe and ZnMgSSe layers on the GaAs substrate (blue laser) or from ZnCdSe and ZnMgCdSe layers on the InP substrate (green laser), as well as from the III–V compounds InGaP and AlGaInP on the GaAs substrate (red laser). At present, the use of a number of the II–VI transparent substrates such as ZnSe, ZnSSe, ZnTe, CdS, and ZnCdS are also being studied [30–34].

The problem is simplified from the technological point of view if 'thinner' potential wells are used [35]. For example, the admissible mismatch for $L_{\rm w} = 5$ nm is $\Delta a/a \leqslant 0.03$. In this case, ternary compounds can be used, for example, the ZnCdSe well between ZnSSe layers on the ZnSe substrate. For such a low value of $L_{\rm w}$, the quantum-size effect is observed, and we are dealing with quantum-well structures. However, because of a limited scope of the paper, we will not analyse here the operation of quantum-well lasers.

The above-mentioned reduction of the lasing threshold by decreasing the resonator losses requires the use of mirror coatings with the high reflection coefficient. It is known that the limiting reflection coefficient of a multilayer interference coating depends to a great extent on the microroughness of the surface on which the coating is deposited. One of such surfaces is the surface of the grown structure. Another surface can be the opposite side of the structure after the removing of the substrate. Other methods for fabricating resonators also exist. The microroughness of the surface is characterised by two parameters: the root-mean-square deviation χ of the microrelief heights with respect to the mean value and the characteristic transverse size ξ determining the mean distance between these heights along the surface. In the most unfavourable case, when $\lambda/N < \xi < d_{\rm e}$, the reflection coefficient of a mirror can be written in the form [17, 36]

$$R = R_0 \exp\left[-(4\pi\chi N/\lambda)^2\right], \tag{13}$$

where R_0 is the reflection coefficient of a mirror deposited on the perfectly plane surface; λ is the radiation wavelength in vacuum; N is the refractive index of the medium from which radiation falls on the surface. When mirrors with losses ~ 0.03 are used, the scattering losses $(4\pi\chi N/\lambda)^2$ should not exceed 0.01. This gives the requirement $\chi < 1$ nm to the surface quality. Such a requirement can be comparatively easily fulfilled for the most technologically mastered III–V compounds, even in the case of rather thick (5–10 μm) heterostructures. However, this problem is still unsolved for multilayer heterostructures based on the II–VI compounds.

Consider now the influence of the mismatch between the gain spectrum and the mode composition of the resonator. The distance between the longitudinal modes of the resonator in a homogeneous active region is described by the expression

$$\Delta\lambda = \frac{\lambda^2}{2N^* L_{\rm c}}, \tag{14}$$

where $N^* = N - \lambda \partial N/\partial\lambda$ is the effective refractive index averaged over the resonator length. Because of the dispersion of the refractive index, the value of N^* can substantially exceed N. The derivative $\partial N/\partial\lambda$ increases upon approaching the energy-gap edge. In the general case, N depends also on the intensity of semiconductor excitation. For CdS and small $L_{\rm c} = 2.2$ μm at room temperature, the value $N^* \approx 6.4$ was obtained [37], which is more than twice as large as $N \approx 2.8$.

In the case of a structure with many potential wells, the value of λ is determined by the energy gap of the well and is located in the region of a weak dispersion of the refractive index $N_{\rm b}^*$ of barrier layers, which occupy the main volume of the resonator [38]. For this reason, the mode interval in such structures is more than twice as large as that in a homogeneous active region. If the mode interval becomes greater than the width of the gain line or even comparable with it, this can cause an additional increase in the lasing threshold or a substantial spatial inhomogeneity of the LS radiation [37]. To obtain the mode frequency that is

constant with an accuracy of 10 % within the LS, the thickness of the active structure should be constant with a high accuracy. For $\lambda = 0.5$ μm, $N^* = 3$ and $L_c = 0.5$ μm, it is necessary that $\Delta L_c/L_c = 1.5 \times 10^{-3}$. This cannot be achieved in practice over a large area of the LS. For this reason, to obtain the required constant characteristics of LSs made of multiwell structures, the value of L_c should be increased at least up to 10 μm. This causes additional complications in the technology of fabrication of LSs from multilayer structures.

4. Radiation power and efficiency of a LCRT

The main characteristic of the LCRT is the efficiency of conversion of the electron-beam energy to the radiation energy. The lasing power can be written in the form

$$P = \eta P_{\rm in}\left(1 - \frac{j_{\rm th}}{j_{\rm in}}\right), \tag{15}$$

where $P_{\rm in}$ and $j_{\rm in}$ are the power and current density of the electron beam; $\eta = \eta_0 k_1 k_3 f_{h\nu}$; $\eta_0 \approx 0.35$ is the limiting theoretical value of the pump conversion efficiency [13]; $k_1 \approx 0.75$ is the coefficient taking into account the fact that a part of the electron-beam energy is not absorbed in the LS but is carried away by reflected electrons and second-emission electrons [39]; k_3 is the coefficient taking into account the nonuniformity of excitation caused by the distribution of the current density in the electron spot; and $f_{h\nu}$ is the radiation output function. Because it is difficult to increase both k_1 and η_0, we can take the product of these parameters equal to 0.27 as the limiting lasing efficiency. Expression (15) is commonly used by assuming that the threshold density of the electron-beam current $j_{\rm th}$, the coefficient k_3, and the output function $f_{h\nu}$ are independent of $j_{\rm in}$. However, this is not the case for electron-beam-pumped lasers. These parameters depend on $j_{\rm in}$ first of all because of a strong heating of the active region during its excitation.

A specific feature of the scanning regime of the LCRT is a substantial inhomogeneity of the temperature along the scanning direction even in the case of uniform excitation in the electron spot. Fig. 2 shows schematically the spatial distribution of the current density, the concentration of nonequilibrium carriers, and temperature in the excited region in the absence of lasing. In this case, the temperature profile changes with changing $j_{\rm in}$. It is obvious that different lasing thresholds can be calculated for each of the temperature profiles. The given threshold cannot be measured because the temperature profile is formed when the pump intensity is different. However, it is this calculated threshold density that should be substituted into expression (15) for measuring the output power. The same is true for the differential efficiency of the laser.

The threshold current density can be calculated as follows. The excited region is divided into small parts, each of them having its own temperature and concentration of nonequilibrium carriers, which correspond to the distribution of the current density in the electron beam and the scanning rate. The gain spectrum is calculated for each of these parts. The gain in each small region is summed with its own weight in accordance with the assumed distribution of the field of an electromagnetic wave in the resonator, giving the overall gain for the given excitation intensity. Then, a

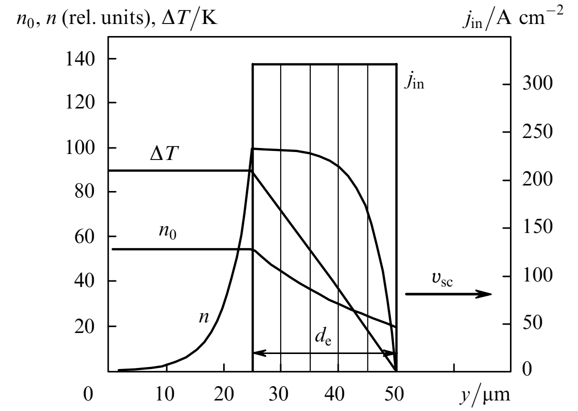

Figure 2. Scheme of the distribution of the current density $j_{\rm in}$, the temperature increment ΔT, the concentration n of nonequilibrium carriers by neglecting stimulated emission, and of the concentration n_0 corresponding to the inversion in the active region; $\upsilon_{\rm sc}$ is the scanning rate.

stationary solution of the wave equation is found for the specified gain profile, specified losses at mirrors and inhomogeneities of the absorption coefficients and refractive indices caused by the given pump intensity.

The experimental study of these processes is hindered because of the smallness of the volume and a large nonuniformity of excitation. The study of the dependence of the lasing spectrum on the scanning rate at low temperature of the LS (80 K) showed that the spectrum broadened to the red, although the broadening was noticeably smaller than that expected due to heating only [22, 40].

The presence of the temperature gradient increases the threshold current density and, hence, the maximum concentration of nonequilibrium carriers in the excited volume. The increase in n results in the red shift of the gain line in accordance with the change in the energy gap (9). The concentration threshold for nonequilibrium carriers in CdS at 80 K is estimated as $n_0 = 8 \times 10^{17}$ cm^{-3}, and the current density used in experiments [22] allows one to produce the concentration $n_{\rm max} \gtrsim 1.2 \times 10^{19}$ cm^{-3}. By substituting these values instead of n in (9), we find that the shift of the long-wavelength edge of the envelope of the lasing spectrum can achieve 20 nm if the threshold concentration of carriers increases up to 1.2×10^{19} cm^{-3} at a low scanning rate. Such a shift was approximately observed in experiments. A large width of the lasing spectrum is caused in this case by the nonuniformity of excitation and the temperature gradient.

The temperature regime of the LCRT with the water-cooled LS was calculated and the influence of heating on the radiation parameters was estimated in [41]. The case of continuos scanning of the LS (of size 3 cm×4 cm) by an electron beam of diameter 25 μm was considered, which is most important in practical applications. The thickness of a heat-sink substrate was 6 mm. The total current was 2 mA, and the electron energy was 50 keV. It was shown that, except the adiabatic heating of the region excited by an electron beam, the background heating should be also taken into account, which is determined by the scanning regime and the cooling system as a whole. The use of the interlaced scanning allows one to avoid the heating of an LS pixel by previous heated lines before the arrival of the electron beam, thereby reducing significantly the background heating.

In the optimal scanning regime (interlaced scanning at the rate $\upsilon_{sc} = 4.2 \times 10^5$ cm s^{-1}), the maximum adiabatic heating was 90 K, while the background heating was 6 K for the CdS LS on a sapphire substrate (neglecting the heating of sapphire with respect to water). The heating of a substrate depends on the velocity and thermal parameters of the cooling liquid and the cooling geometry. Estimates have shown that this heating can be less than 10 K. The influence of the adiabatic and background heating on the LCRT parameters is different. The adiabatic heating occurs only in the excited region and has no time to propagate into the passive region of the resonator during lasing, whereas the background heating covers the entire volume of the semiconductor, thereby affecting the resonator losses to a greater extent.

The output function $f_{h\nu}$ can written in the form

$$f_{h\nu} = \frac{|\ln R_2|}{|\ln(R_1 R_2)| + 2\alpha L_c}. \qquad (16)$$

The resonator losses $2\alpha L_c$ can be estimated taking into account the difference between the absorption coefficients of the active and passive regions [see (10)], as well as losses caused by scattering of radiation by mirrors. The losses in the active region are mainly determined by absorption of radiation by free carriers. The absorption coefficient for undoped GaAs is $\alpha_{fc} = Kn$, where $K = 10^{-17}$ cm^2 [42]. For $n = 10^{19}$ cm^{-3}, we have a rather large absorption coefficient $\alpha_{fc} = 100$ cm^{-1}. If absorption is accompanied by scattering by optical phonons [43], then $\alpha_{fc} \sim \lambda^{2.5}$, and we can expect that $\alpha_{fc} = 30$ cm^{-1} for CdS. By estimating losses of this type, we should also take into account that the number of optical phonons in the region excited by an electron beam can be higher than their equilibrium value at the given temperature of the crystal. Therefore, upon heating of the active region, losses in it will increase faster than the threshold concentration of nonequilibrium carriers.

Losses in the passive region of the resonator are determined by the absorption edge of the unexcited crystal. Of course, the passive region can be partially bleached, but in this case, absorption by free carriers will increase. The absorption coefficient of the unexcited crystal at room temperature is well described by the empirical Urbach rule

$$\alpha_p = \alpha_0 \exp\left(-\vartheta\,\frac{E_U - \hbar\omega}{kT}\right), \qquad (17)$$

where $\alpha_0 = 1.5 \times 10^9$ cm^{-1}, $\vartheta = 2.43$, $E_U = 2.572$ eV for CdS at 300 K [44]. By substituting into (17) the energy of photons (522 – 523 nm) emitted by the CdS LS at room temperature, we obtain $\alpha_p \approx 10$ cm^{-1}. Somewhat greater values of α_p in this spectral region were obtained in [45]. The estimate of internal losses made from the dependence of the output power from the reflection coefficient of mirrors gives 25 – 30 cm^{-1} [20].

Consider now the dependence of losses in the passive region on the crystal temperature. Fig. 3 shows the dependence of the lasing spectrum of the CdS LS on the thermostat temperature T upon scanning along the line at a rate of 4×10^5 cm s^{-1} and a pulse repetition rate of 50 Hz (pulsed scanning) for a current of 0.8 mA and a 50-keV electron beam. Under these conditions, the background heating can be neglected and the adiabatic heating of the active region can be minimised. The temperature shift of the maximum of the spectrum envelope can be described by the expression $\hbar\omega = (2.522 - 5.125 \times 10^{-4} T)$ eV, where T is in kelvins. By substituting this expression into (17) and differentiating it, we find that losses should increase with temperature approximately five times faster than the temperature.

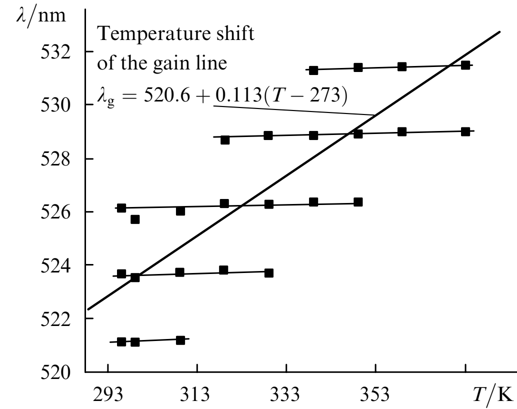

Figure 3. Dependences of the positions of modes (points) and the maximum of the envelope of the lasing spectrum (a straight line) on the thermostat temperature for the CdS LS.

The analysis performed above shows that the resonator losses should increase with the crystal temperature. This will inevitably reduce the output function of the laser and its differential efficiency as a whole. Fig. 4 shows the typical dependence of the differential efficiency of the laser on the thermostat temperature, which was obtained for CdS LS in the pulsed scanning excitation regime. One can see that the efficiency strongly decreases above room temperature. The experimental points are well described by the empirical curve $\eta = 0.067/\{1 + 0.2\exp[(T - 290)/30]\}$ [41]. By comparing this curve with expression (16) for the output function, we find that the resonator losses increase exponentially with temperature for a low characteristic temperature 30 K.

So far, it is not clear why the maximum efficiency of the laser is less than 7 %, which is substantially lower than the limiting value 27 %. The limiting efficiency (26.5 %) was

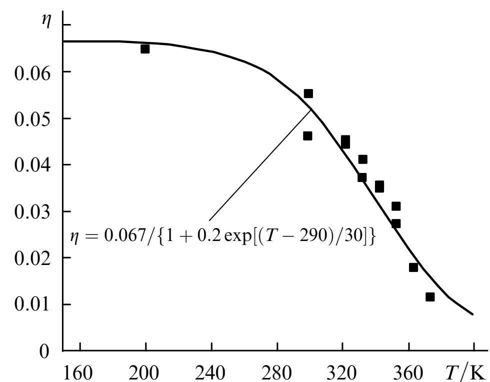

Figure 4. Temperature dependence of the differential efficiency for the CdS LS.

achieved experimentally at liquid helium temperature in a ductile CdS crystal transversely pumped by an electron beam [46]. In this case, the lasing threshold was extremely low ($j_{\rm th} = 0.02$ A cm^{-2}). A quite high differential efficiency (20 %) was achieved at room temperature by longitudinal pumping CdS crystals by broad 200 – 300-eV electron beams [47]. The lasing efficiency of 14% was obtained upon longitudinal pumping of variband AlGaAs structures by a focused 75-keV electron beam [48]. However, the lasing efficiency of the same structures pumped by 50-keV electrons was only 8.8 %.

It follows from the analysis of the known data that the necessary condition for obtaining a high lasing efficiency is a sufficiently low lasing threshold, and the better results were obtained upon uniform pumping. The theory shows that the transverse distribution of the electromagnetic field at the lasing threshold is considerably narrower than the distribution of the current density in the electron spot [17]. Above the lasing threshold, the transverse dimensions of the electromagnetic field increase, for example, due to excitation of modes with a higher transverse index. However, a fraction of nonequilibrium carriers at the periphery of the electron spot do not contribute to lasing. It seems that the consideration of the inhomogeneity can partially explain a relatively low lasing efficiency at room temperature.

Another technical feature of pumping by a sharply focused electron beam is a change in the electron-beam diameter with increasing current, which cannot be virtually eliminated. This is caused by the Coulomb repulsion between like charges at the stage of the beam formation in an electron gun. The lower the accelerating voltage, the stronger the effect. Fig. 5 shows the dependences of the lasing threshold with respect to the current and radiation power on the electron energy for three different LSs, emitting in different spectral regions. A substantial increase in the threshold current and a decrease in the output power at low electron energies are caused mainly by an increase in the electron-beam diameter.

Consider now the effect of the adiabatic heating on the watt – ampere characteristic. We assume that the diameter $d_{\rm e}$ is independent of the current, and therefore $j_{\rm th}$ can be replaced by $I_{\rm th}$ in expressions (8) and (15). Then, we substitute the current $I_{\rm th} = I_{\rm th}(T_1)(1 + \beta I/T_0)$ instead of $j_{\rm th}$ in expression (15). Here, we took the first term in the expansion of the exponential in expression (8) and replaced $T - T_1$ by βI. Expression (15) can be transformed in this case as

$$P = \eta P_{\rm in}\left(1 - \frac{I_{\rm th}(T_1)\beta}{T_0}\right) \times\left[1 - \frac{I_{\rm th}(T_1)}{I}\left(1 - \frac{I_{\rm th}(T_1)\beta}{T_0}\right)^{-1}\right]. \quad (18)$$

One can see that, if the adiabatic heating does not substantially affect the parameter η, then the watt – ampere characteristic is linear, but its slope decreases by a factor of $1 - I_{\rm th}(T_1)\beta/T_0$, while the threshold current density increases by the same factor. For the case considered above ($I = 2$ mA, the average heating $\Delta T = 45$ K), we have $\beta = 22.5$ K mA^{-1}. For $T_0 = 140$ K and $I_{\rm th} = 0.2$ mA, we obtain the relative change in the slope of the watt – ampere characteristic equal to 0.97. If we substitute, however, into the dependence $\eta(T(j_{\rm th}))$ the temperature rise caused by adiabatic heating, then the watt – ampere characteristic will be nonlinear. Fig. 6 shows the dependences of the output power on the electron-beam power for three LSs emitting in different spectral regions. These characteristics were obtained upon pulsed scanning under the conditions close to the calculations (the maximum temperature increment was 90 K). The LS emitting in the blue region was made of ZnSSe single crystals, which were recently grown from a vapour phase [49]. One can see from Fig. 6 that the power characteristics are virtually linear. This means that losses in the active medium are not dominant. Another conclusion is that the adiabatic heating does not limit the output power when the scanning rate is properly chosen, whereas the background heating can substantially reduce

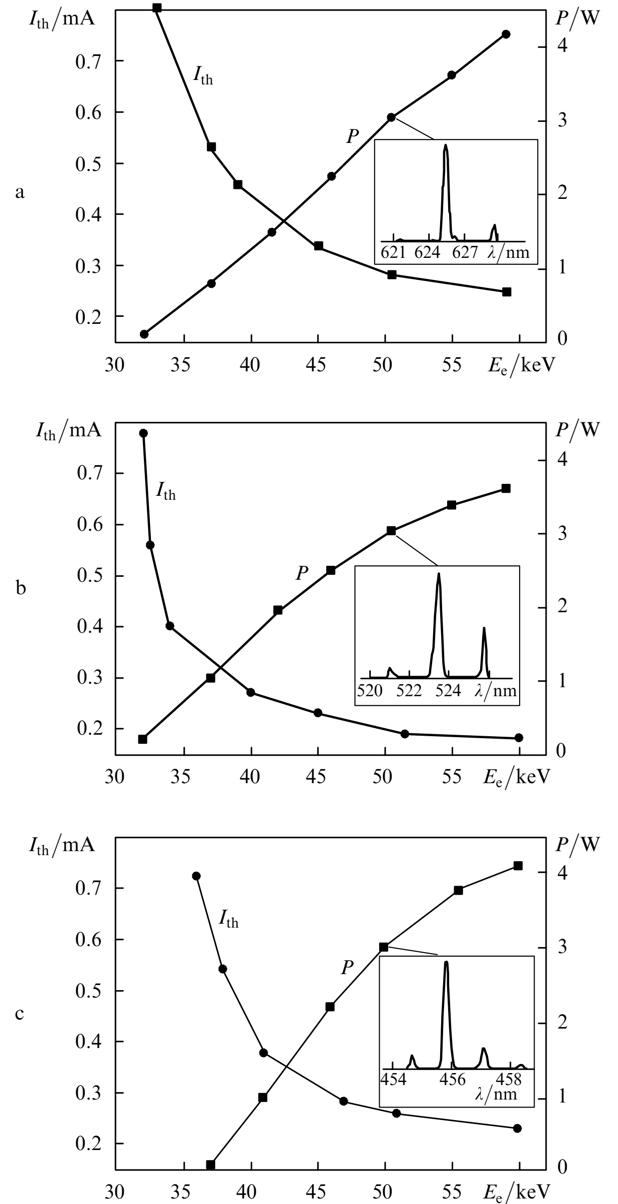

Figure 5. Dependences of the threshold current and the output power on the electron energy for the current $I = 1.6$ mA at room temperature for three different LSs emitting in the red (a), green (b), and blue (c) spectral regions. Inserts show lasing spectra for $E_{\rm e} = 50$ keV.

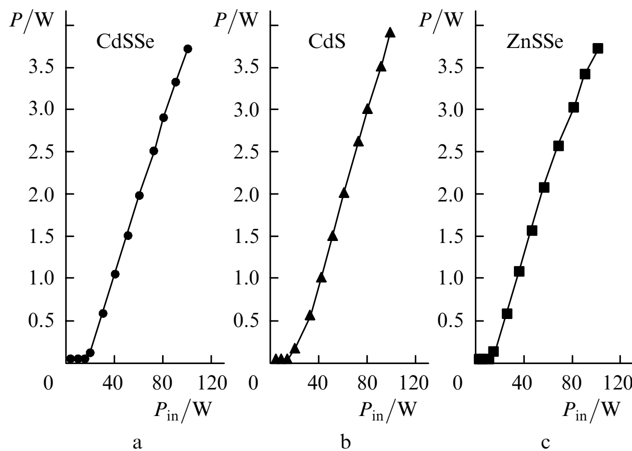

Figure 6. Dependences of the output power on the 50-keV electron-beam power at room temperature for three different LSs emitting in the red (a), green (b), and blue (c) spectral regions.

the output power and efficiency of the laser, as follows from Fig. 4.

The temperature regime of the LS is virtually independent of the active-region material. The same is true for the effects related to a change in the electron-beam diameter. However, the achievement of a high output function for the LS made of a quantum-size structure is a more complicated problem because this requires the use of a higher-Q resonator. A relatively high output power of 2.2 W has been achieved so far in a structure with 150 quantum wells [50]. Recently, a ZnCdSe/ZnSe laser with 15 quantum wells grown on the ZnSe substrate was created. However, its output power was only 0.3 W [51].

5. Conclusions

Although not little has been already done for practical applications of LCRTs, many problems still remain to be solved. A substantial improvement of the LCRT characteristics at room temperature achieved recently due to the improvement of the technology of LS manufacturing from single crystals allows one to hope that this way will lead to the creation of the first commercial television projector with a high resolution and the radiation flux of 3000–5000 lm. A more promising epitaxial technology can be used only after solving a number of important physical and technological problems, which require the considerable financial support.

The studies of LCRTs have been performed for years under the supervision of Nikoli Gennadievich Basov. The authors devote this work to his memory.

Acknowledgements. This work was supported by the complex programme 'Low-Dimensional Quantum Structures' of the Presidium of RAS, the federal programme 'Physics of Solid Nanostructures', the Russian Foundation for Basic Research (Grant No. 01-02-16409), programme 'Leading Scientific Schools' (Grant No. 00-15-96624), and the Principa LightWorks Inc., CA.

References

1. Basov N.G., Bogdankevich O.V., Nasibov A.S. USSR Inventor's Certificate No. 270100; *Byull. Izobret.*, (16) (1970).
2. Parkard I.R., Tait W.C., Dierssen G.H. *Appl. Phys. Lett.*, **19**, 338 (1971).
3. Basov N.G., Bogdankevich O.V., Nasibov A.S., Pechenov A.N., Kozlovsky V.I., Shapkin P.V., Kamenev V.M., Pochernyaev V.M., Papusha P.V. *Dokl. Akad. Nauk SSSR*, **205**, 72 (1972).
4. Honda T., Sakaguchi T., Koyama F., Iga K., Inoue K., Munekata H., Kukimoto H. *J. Crystal Growth*, **159**, 595 (1996).
5. Georgobiani A.N., Sheikman M.K. (Eds) *Fizika soedinenii A_2B_6* (Physics of the II–VI Compounds) (Moscow: Nauka, 1986).
6. Kozlovsky V.I., Nasibov A.S., Reznikov P.V. *Fiz. Tverd. Tela*, **13**, 1348 (1979).
7. Tait W.C., Packard J.R., Dierssen G.H., Campbell D.A. *J. Appl. Phys.*, **38**, 3035 (1967).
8. Benoit C. a la Guillaume, Debever J.M., Salvan F. *Phys. Rev.*, **177**, 567 (1969).
9. Lysenko V.G., Revenko V.I., Tratas T.G., Timofeev V.B. *Zh. Eksp. Teor. Fiz.*, **68**, 335 (1975).
10. Ding J., Jeon H., Ishihara T., Hagerott M., Nurmikko A.V. *Phys. Rev. Lett.*, **69**, 1707 (1992).
11. Kozlovsky V.I., Nasibov A.S., Pechenov A.N., Popov Yu.M. *Kvantovaya Elektron.*, **6**, 189 (1979) [*Sov. J. Quantum Electron.*, **9**, 104 (1979)].
12. Mott N.F. *Phil. Mag.*, **6**, 287 (1961).
13. Popov Yu.M. *Trudy FIAN*, **37**, 3 (1965).
14. Kozlovsky V.I., Nabiev R.F., Nasibov A.S., Poluektov I.A., Popov Yu.M. *Kvantovaya Elektron.*, **9**, 806 (1982) [*Sov. J. Quantum Electron.*, **12**, 505 (1982)].
15. Nabiev R.F., Popov Yu.M. *Trudy FIAN*, **202**, 7 (1991).
16. Haug H., Koch S.W. *Phys. Rev. A*, **39**, 1887 (1989).
17. Ulasyuk V.N. *Kvantoskopy* (Quantoscopes) (Moscow: Radio i Svyaz', 1988).
18. Bogdankevich O.V., Darznek S.A., Eliseev P.G. *Poluprovodnikovye lazery* (Semiconductor Lasers) (Moscow: Nauka, 1976).
19. Kozlovsky V.I., Reznikov P.V. *Trudy FIAN*, **202**, 34 (1991).
20. Kozlovsky V.I., Nasibov A.S., Reznikov P.V. *Kvantovaya Elektron.*, **8**, 2493 (1981) [*Sov. J. Quantum Electron.*, **11**, 1522 (1981)].
21. Kozlovsky V.I., Nasibov A.S., Popov Yu.M., Reznikov P.V., Skasyrsky Ya.K. *Proc. SPIE Int. Soc. Opt. Eng.*, **2407**, 313 (1995).
22. Kozlovsky V.I. *A Study of Electron-Beam-Pumped Semiconductor Lasers*. Cand. Diss. (Moscow, FIAN, 1979).
23. Colak S., Khurgin J., Seemungal W., Hebling A. *J. Appl. Phys.*, **62**, 2633 (1987).
24. Khalfin V.B., Garbuzov D.S., Davidyuk N.Yu. *Fiz. Tekh. Poluprovodn.*, **10**, 1490 (1976).
25. Gribkovskii V.P. *Poluprovodnikovye lazery* (Semiconductor Lasers) (Minsk: Izd. Minsk Univ., 1988).
26. Eliseev P.G. *Vvedenie v fiziku inzhektsionnykh lazerov* (Introduction to the Physics of Injection Lasers) (Moscow: Nauka, 1983).
27. Bogdankevich O.V., Bryunetkin B.A., Darznek S.A., Zverev M.M., Ushakhin V.A. *Kvantovaya Elektron.*, **5**, 2035 (1978) [*Sov. J. Quantum Electron.*, **8**, 1138 (1978)].
28. Kozlovsky V.I., Sadofyev Yu.G. *J. Vac. Sci. Technol. B*, **18**, 1538 (2000).
29. Parbrook P.J., Henderson B., O'Donnell K.P., Wright P.J., Cockayne B. *J. Crystal Growth*, **117**, 492 (1992).
30. Kozlovsky V.I., Trubenko P.A., Dianov E.M., Korostelin Yu.V., Skasyrsky Yu.K., Shapkin P.V. *Kvantovaya Elektron.*, **25**, 305 (1998) [*Quantum Electron.*, **28**, 294 (1998)].
31. Kozlovsky V.I., Nasibov A.S., Pechenov A.N., Popov Yu.M., Reznikov P.V. *Kvantovaya Elektron.*, **4**, 2246 (1977) [*Sov. J. Quantum Electron.*, **7**, 1283 (1977)].
32. Kozlovsky V.I., Krysa A.B., Korostelin Yu.V., Sadofyev Yu.G. *J. Crystal Growth*, **214/215**, 35 (2000).
33. Kozlovsky V.I., Martovitsky V.P., Skasyrsky Ya.K., Sadofyev Yu.G., Turyansky A.G. *Phys. Stat. Sol. (b)*, **229**, 63 (2002).
34. Kozlovsky V.I., Martovitsky V.P., Sannikov D.A., Kuznetsov P.I., Yakushcheva G.G., Jitov V.A. *J. Crystal Growth*, **248**, 62 (2003).

35. Kozlovsky V.I., Lavrushin B.M. RF Patent No. 2056665; *Byull. Izobret*., (8) (1966); EP 0696094 B1 Bul. 1999/41; US Patent 5687185.
36. Troubenko P.A., Kozlovsky V.I., Yao T., Korostelin Y.V., Roddatis V.V. *J. Crystal Growth*, **227/228**, 699 (2001).
37. Kozlovsky V.I., Nasibov A.S., Reshetov V.I. *Kvantovaya Elektron*., **5**, 2624 (1978) [*Sov. J. Quantum Electron*., **8**, 1477 (1978)].
38. Kozlovsky V.I., Trubenko P.A., Skasyrsky Y.K. *Laser Phys*., **8**, 1068 (1998).
39. Bogdankevich O.V., Donskoi E.N., Kovalenko V.A., Panitkin Yu.G., Tarasov M.D. *Kvantovaya Elektron*., **10**, 2236 (1983) [*Sov. J. Quantum Electron*., **13**, 1453 (1983)].
40. Kozlovsky V.I., Nasibov A.S., Pechenov A.N., Reznikov P.V., Skasyrsky Ya.K. *Kvantovaya Elektron*., **5**, 487 (1978) [*Sov. J. Quantum Electron*., **8**, 281 (1978)].
41. Kozlovsky V.I., Kumykov Kh.Kh., Malyshev I.V., Popov Yu.M. *Kvantovaya Elektron*., **32**, 297 (2002) [*Quantum Electron*., **32**, 297 (2002)].
42. Gasey N.C. Jr., Panise M.B. *Heterostructure Lasers, Part A* (New York: Academic Press, 1978; Moscow: Mir, 1981) Vol. 1.
43. Pankove J.I. *Optical Processes in Semiconductors* (Englewood Cliffs: Prentice–Hall, N.J., 1971; Moscow: Mir, 1973).
44. Gnatenko Yu.P., Kurik M.V. *Fiz. Tverd. Tela*, **12**, 1143 (1970).
45. Akhekyan A.M., Kozlovsky V.I., Korostelin Yu.V., Reznikov P.V., Tikhonov V.G., Shapkin P.V. *Trudy FIAN*, **202**, 128 (1991).
46. Hurwitz C.E. *Appl. Phys. Lett*., **9**, 420 (1966).
47. Daneu V., DeGloria D.P., Sanchez A., Tong F., Osgood R.M. Jr. *Appl. Phys. Lett*., **49**, 546 (1986).
48. Gubarev A.A., Lavrushin B.M., Nabiev R.F., Nasibov A.S., Sypchenko M.N., Popov Yu.M. *Trudy FIAN*, **202**, 158 (1991).
49. Korostelin Yu.V., Kozlovsky V.I. *Phys. Stat. Sol. (b)*, **229**, 5 (2002).
50. Kozlovsky V.I., Shcherbakov E.A., Dianov E.M., Krysa A.B., Nasibov A.S., Trubenko P.A. *J. Crystal Growth*, **159**, 609 (1996).
51. Kozlovsky V.I., Korostelin Yu.V., Popov Yu.M., Skasyrsky Ya.K., Sadofyev Yu.G. *Phys. Stat. Sol. (b)*, **229**, 1033 (2002).